

# Analysis of Received Power via RIS in Near Field LOS Channels

Joonas Kokkonen

Centre for Wireless Communications (CWC), University of Oulu, P.O. Box 4500, 90014 Oulu, Finland

Email: joonas.kokkonen@oulu.fi

**Abstract**—The reconfigurable intelligent surfaces (RISs) are expected to be a cheap way to extend service areas of base stations. This is especially promising welcome in the millimeter wave and THz bands (from 30 GHz to +1 THz) where base station coverage is expected to be modest and suffer greatly from blockages. As the RISs can be potentially large (physically and via number of sub-elements), there is a good chance that a user is in the near field of RIS. This paper considers RIS near field propagation and achievable power levels close to these surfaces. Ideal energy levels are looked into among with the impact of beamforming and beam squinting and human safety issues are briefly analyzed. It is shown that the achievable received power in the near field are very good, but the beam squinting may have a significant impact on the received power and frequency response. We also conclude that RISs are safe for humans even at close proximity due to relatively large channel losses in the reflected channels and hence low power densities in the air.

## I. INTRODUCTION

The future 6G and beyond systems are expected to widely utilize millimeter wave band (30 – 300 GHz) and THz frequencies (+300 GHz) for close range communications. The high frequency bands give possibility to increase data rates primarily by brute force manner by having space for very high communication bandwidths [1], [2]. However, these frequencies also suffer from very high path losses that limit the achievable communications ranges [3]. Blockage is particularly large issue as the high frequencies tend not to penetrate materials very easily. This is an issues in densely constructed areas, such as urban areas and indoor locations. An obvious solution is to densify the network to decrease outage areas and increase the overall network capacity and throughput. The problem becomes with the cost that extremely dense network imposes on the network operator.

A potential solution and intensely studied topic during the past years have been reconfigurable intelligent surfaces (RISs), also known as large intelligent surfaces (LISs) or intelligent reflecting surfaces (IRSs). The basic assumption of RISs considers them as surfaces formed of large numbers of sub-elements that can control the phase (and amplitude) of the incoming signals. By adjusting the phase of the reflected wave, RISs can produce anomalous reflections that can be used to locally control the radio environment. There is a comprehensive survey on RISs, different types of RISs, and their modeling in [4]. While the most of the papers consider RISs fully passive in a sense that they do not have any radio frequency (RF) chains in them, some works also consider

active RISs where few RF chains are utilized to help with, e.g., channel estimation [5].

In this work we analyze the near field propagation of large RISs. In order for the RIS to be able to gather sufficient amount of energy for redirection, it has to be physically large. Depending on the frequency and RIS gain requirements, the number of antenna elements has to be large as well. Large physical apertures cause the near field of the antenna array/reflecting surface to extend far. In certain scenarios, such as dense urban areas or indoor location this may force the users to be in the near field of the antenna/surface. Our aim here is to analyze the achievable gain in the near field of the RISs and estimate the impact of basic beamforming techniques on the receiver power. These include the analysis of the linear phase beamforming (LPBF) and near field focusing (NFF) on the received power and impact of the beam squinting on the received power and frequency response. Lastly, we consider some health limits for large RISs and show that the channel losses tend to be so large that the RISs impose no health concern for humans except in special circumstances.

We analysed the near field propagation of large antenna arrays in the past in [6]. This work extends that to context of RIS. The gain properties of RISs were studied in various works, including in ours in [7]. We also studied the RIS interference by means of stochastic geometry in [8]. There many very interesting channel modeling related works on RISs [9]–[13] considering different modeling aspects. In this paper we mostly focus on the near field and as a new new aspect the energy densities close to RISs with near field focusing techniques to analyse safety of RISs. The basic channel models herein are essentially similar to the literature with some differences coming from assumptions behind the models.

## II. SYSTEM AND PROPAGATION MODELS

### A. System Model

The system model is shown in Fig. 1. It consists a transmitter (Tx), a RIS, and a receiver (Rx). Due to focus on the near field propagation, we assume all the channel to be line-of-sight (LOS) as this enables near field focusing, which is better covered in the next section. Unless otherwise noted, Tx is assumed to be located directly in front of the RIS in order to simplify the Tx–RIS channel. This channel is still important since it feeds the energy to RIS for redirection. The Rx position is changed to see the behavior of Tx–RIS–Rx compound channel as a function of the RIS angle.

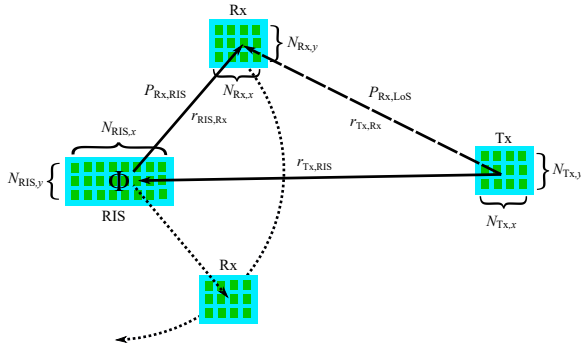


Fig. 1. System model considered in this paper.

To fix the total link distance, we surround the RIS with possible Rx positions. This way we can see the impact of the RIS beamforming on the received signal, while keeping the distances fixed. In the results, we focus on received power at Rx, but also we briefly look into energy density in the air to determine if large RISs can cause harmful energy densities in the near field. In this case, we assume the Tx and the Rx to be directly in front of the RIS to eliminate the beam squint to give as pessimistic worst case energy densities.

We assume that the Tx and Rx antennas are arrays formed of the isotropically radiating antenna elements. We also assume that the RIS is formed of hemispherically radiating antenna elements. That is, RIS elements scatter the power equally in all directions towards the reflection side of the surface, but it does not radiate to the backside of the RIS. Spherical assumptions on the RISs are often criticized due to being too simple, but in reality, e.g., a patch antenna group has relatively spherical radiation pattern as long as the elements are small [11]. This is especially the case when element size is in the order of  $\lambda/2$ , where  $\lambda$  is the wavelength. Furthermore, at high frequencies the usual  $\lambda/2$  assumption results in very tiny RISs, even with very large numbers of antenna elements. Hence, more reasonable assumption is to make the individual elements slightly larger. We mostly use  $2\lambda$ -sized elements to gather more energy. This makes the spherical radiation assumption a bit weaker, since in the real world such patch array will start to emphasize specular reflection direction [11]. This will be better analyzed and discussed in a future publication where we show results for RIS propagation via ray tracing simulations.

### B. Basic Propagation Models

Two of the most important losses in sub-THz are the free space path loss (FSPL) and molecular absorption loss, respectively given by their channel gains as

$$\sigma_{\text{FSPL}}(r, f) = \frac{c^2}{(4\pi r f)^2}, \quad (1)$$

and

$$\sigma_{\tau}(r, f) = \exp(-\kappa_a(f)r), \quad (2)$$

where  $c$  is the speed of light,  $f$  is the frequency,  $r$  is the link distance, and  $\kappa_a(f)$  is the absorption coefficient, which can be modeled, e.g., like shown in [3] or [14]. It is important

to understand that the free space loss consist both signal expansion gain ( $1/4\pi r^2$ ) and antenna aperture term ( $c^2/4\pi f^2$ ) as RISs do not receive the signals. Hence, signal reflected via the RISs also do not have the above aperture loss, but the physical area of the RIS determines the amount of reflected energy.

In this paper, we consider three different types of links: LOS link between Tx and Rx, Tx-Rx link via RIS, and energy density ( $\text{W}/\text{m}^2$ ) through certain averaging area  $A_{\text{ave}}$  with and without RIS. The individual link gains in these cases are as follows. The direct LOS link gain is directly

$$\begin{aligned} \sigma_{\text{LOS}}(r_{\text{LOS}}, f) &= \sigma_{\text{FSPL}}(r_{\text{LOS}}, f) \sigma_{\tau}(r_{\text{LOS}}, f) \\ &= \frac{c^2}{(4\pi r_{\text{LOS}} f)^2} e^{-\kappa_a(f)r_{\text{LOS}}}, \end{aligned} \quad (3)$$

where  $r_{\text{LOS}}$  is the LOS link distance. Link gain between Tx and RIS is

$$\sigma_{\text{Tx,RIS}}(r, f) = \frac{A_{\text{RIS}} \exp(-\kappa_a(f)r_{\text{Tx,RIS}})}{4\pi r_{\text{Tx,RIS}}}, \quad (4)$$

where  $r_{\text{Tx,RIS}}$  is the Tx-RIS link distance and  $A_{\text{RIS}}$  is the effective energy capturing area for RIS. Link gain between RIS and Rx is

$$\sigma_{\text{RIS,Rx}}(r, f) = \frac{c^2 \exp(-\kappa_a(f)r_{\text{RIS,Rx}})}{8\pi^2 r_{\text{RIS,Rx}}^2 f^2}, \quad (5)$$

assuming that the RIS reflects hemispherically (RIS is not transparent) and hence the energy expansion term is  $1/2\pi r^2$ , where  $r_{\text{RIS,Rx}}$  is the link distance between RIS and Rx. Finally, if we consider a generic area  $A_{\text{ave}}$  for an average power flow, the link gain from RIS to that area is

$$\sigma_{\text{RIS},A_{\text{ave}}}(r, f) = \frac{\exp(-\kappa_a(f)r_{\text{RIS},A_{\text{ave}}})}{2\pi r_{\text{RIS},A_{\text{ave}}}^2}, \quad (6)$$

where  $r_{\text{RIS},A_{\text{ave}}}$  is the distance between RIS and the area  $A_{\text{ave}}$ . In the further when calculating average energy density over unit area, we omit  $A_{\text{ave}}$  due to effective division with the averaging area. By assuming that the radiation flow through the area is roughly uniform, this yields the power density through a unit area. This is not always the case if the RIS has very large number of elements and is able to focus the energy on very small area. This will be shown in the numerical results.

## III. RIS LOS PROPAGATION MODELS

### A. Total Channel Responses

Throughout the derivations it is assumed that the antenna element do not have directivities, disregarding the RIS as per previous section. Otherwise those need to be included in below. Also, we assume that the RIS does not absorb any energy and the Tx and Rx do not do any amplitude tapering, etc. Therefore, we only take into account the phases of the antennas, but the amplitudes could be added if one would like to, e.g., decreases side lobe levels.

Taking into account the channel gains above, the Tx and Rx antennas, and the transmit power, the LOS channel becomes the familiar [3]

$$h_{\text{LOS}}(r_{\text{LOS}}) = \int_B P_{\text{Tx}}(f) G_{\text{Tx}} G_{\text{Rx}} \frac{c^2 \exp(-\kappa_a(f) r_{\text{LOS}})}{(4\pi r_{\text{LOS}} f)^2} df, \quad (7)$$

assuming that the transmit power  $P_{\text{Tx}}(f)$  captures the frequency response of the transmitted signal (if equal power distribution across frequencies:  $P_{\text{Tx}}(f) = P_{\text{Tx}}/W$ , where  $W$  is the bandwidth of the Tx signal), where  $B$  is the frequency band for integration,  $\kappa_a(f)$  is the absorption coefficient at frequency  $f$  (usually can be omitted if short link distance or if transmission frequencies are not close to absorption lines), and  $G_{\text{Tx}}$  and  $G_{\text{Rx}}$  are the Tx and Rx antenna gains. In the case of an array, in ideal case these correspond to the number of antenna elements:  $G_{\text{Tx}} = N_{\text{Tx}}$  and  $G_{\text{Rx}} = N_{\text{Rx}}$ , where  $N_{\text{Tx}}$  and  $N_{\text{Rx}}$  are the number of antenna element in Tx and Rx arrays.

The Tx-RIS-Rx received power is obtained as

$$\begin{aligned} h_{\text{RIS}} &= \int_B P_{\text{Tx}}(f) \left| \frac{1}{\sqrt{N_{\text{Tx}} N_{\text{RIS}} N_{\text{Rx}}}} \sum_{i=1}^{N_{\text{Tx}}} \sum_{l=1}^{N_{\text{RIS}}} \sum_{k=1}^{N_{\text{Rx}}} \Theta_i \Xi_l \Phi_k \right. \\ &\quad \times \exp(-j2\pi c(r_{i,l} + r_{l,k})/f) \sqrt{\frac{c^2 A_{\text{RIS}}}{32\pi^3 f^2 r_{\text{Tx,RIS}}^2 r_{\text{RIS,Rx}}^2}} \\ &\quad \left. \times \exp(-\frac{1}{2} \kappa_a(f) [r_{\text{Tx,RIS}} + r_{\text{RIS,Rx}}]) \right|^2 df, \end{aligned} \quad (8)$$

where  $\Theta_i$ ,  $\Xi_l$ , and  $\Phi_k$  are the phases of the Tx, RIS, and Rx, respectively, and those are also given as  $\Theta_i = a_i e^{-j\theta_i}$ , where  $a_i$  is the amplitude of the  $i$ th Tx antenna element (assumed to be unit as per above assumptions) and  $\theta_i$  is the phase shift of the  $i$ th Tx antenna element. With the same logic as for Tx, the RIS and Rx amplitude and phase are:  $\Xi_l = a_l e^{-j\xi_l}$  and  $\Phi_k = a_k e^{-j\phi_k}$ . Furthermore, term  $\exp(-j2\pi c(r_{i,l} + r_{l,k})/f)$  accounts for the linear phase shift of the signal from antenna element to antenna element.

In the real world, jointly optimizing  $\Theta_i$ ,  $\Xi_l$ , and  $\Phi_k$  is a very challenging problem, especially in more complex channels and potentially in multiuser setting. In an ideal case where the above phases sum constructively, the received power becomes

$$\begin{aligned} h_{\text{RIS}} &= \int_B P_{\text{Tx}}(f) G_{\text{Tx}} G_{\text{Rx}} G_{\text{RIS}} \\ &\quad \times \frac{\exp(-\kappa_a(f) [r_{\text{Tx,RIS}} + r_{\text{RIS,Rx}}]) c^2 A_{\text{RIS}}}{32\pi^3 f^2 r_{\text{Tx,RIS}}^2 r_{\text{RIS,Rx}}^2} df. \end{aligned} \quad (9)$$

### B. Beamforming in Near and Far Fields

The phase terms  $\Theta_i$ ,  $\Xi_l$ , and  $\Phi_k$  play an important role in achieving the maximum gain possible for the antenna. This means in practice perfect constructive sum at the observation point. The most used beam steering method for uniform linear or planar antenna arrays (ULAs or UPAs) in the literature is the linear phase beam steering, which gives the maximum gain in

the far field of the antenna. It is defined for ULA (per antenna) as

$$\delta_{\text{LPBF}} = e^{j \frac{2\pi}{\lambda} d(n-1) \sin(\alpha)}, \quad (10)$$

with very similar expression for UPA, where  $d$  is the separation of the antenna elements,  $n$  is the index of the antenna element in the array, and  $\alpha$  is the steering angle. The biggest issue of the LPBS comes in the near field. The LPBS works very well when the channel imposes constant phase change on the signal across the antennas, that is, in RIS case above, the linear phase shifts  $\exp(-j2\pi c(r_{i,l} + r_{l,k})/f)$  is approximately equal over all antennas. This is not the case in the near field. Hence, the ideal beamformer there is given by the exact linear phase shifts from antenna to antenna propagation

$$\delta_{\text{NFF}} = e^{j2\pi c(r_{i,l} + r_{l,k})/f}. \quad (11)$$

We can see that this exactly zeros the linear phase shifts, and hence, it focuses the energy on the Rx. In the far field NFF gives the same response as LPBF since the distances from antenna elements to far away are equal. The great downside of NFF is the need for one extra degree of freedom. To calculate the phases, one does not only require the two angle (azimuth/elevation), but distance as well. This is a great challenge for real systems where exact locations are not easy to obtain from pure channel data on millimeter level.

On top of these, beam squinting will become an issue with both of the above steering methods. This is caused by the need to design the beamforming about some center frequency. There are ways to compensate the beam squinting at Rx and Tx, e.g., with time delay based solutions. With RISs, this is more difficult due to lack of RF chains. We also analysed the beam squinting in the past with ULAs and UPAs [15]. In this work, we are mostly interested in the beam squinting in the near field. However, as it will be seen in the results, it does not matter if one is in far or near field. The beam squinting at RIS will impose additional losses on high bandwidth signals.

### C. Energy Density in Air

When a user is close to a large RIS, there is a theoretical chance to impose the user on very large local energy densities. The total energy is bound by the transmit power, but locally there can be hot spots that exceed the recommendations. We follow the recommendation by IEEE C95.1-2019 [16] that gives the following exposure reference levels (ERLs) for local area exposure (above 6 GHz, unrestricted environment):  $ERL = 55 f_G^{-0.177} \text{ W/m}^2$  and  $ERL = 110 f_G^{-0.177} \text{ W/m}^2$  for local area exposure with 4 cm<sup>2</sup> averaging area and small area exposure with 1 cm<sup>2</sup> averaging area, respectively. At the considered 140 GHz band, these correspond to approximately 22.9 W/m<sup>2</sup> and 45.9 W/m<sup>2</sup>. These are quite high limits, especially for transmit power limited high frequency devices. However, these are limits per square meter, the effective exposure per square meter can be substantially high if energy is concentrated on small area, e.g., with a very large RIS. Given above assumptions, the energy density via RIS link can

TABLE I  
TYPICAL SIMULATION PARAMETERS

Parameter	Value
Center frequency	140 GHz
Bandwidth	2 and 10 GHz
Transmit power	1 W
Tx size	8-by-8 array
Rx size	8-by-8 array
RIS size	32-by-32 array
Rx and Tx element sizes	$\lambda/2$ -by- $\lambda/2$
RIS element size	$2\lambda$ -by- $2\lambda$
Tx distance from RIS	15 m
Rx distance from RIS	2, 5, and 10 m

be calculated as

$$E_d = \frac{1}{A_{\text{ave}}} \int_A \int_B P_{\text{Tx}}(f) \left| \frac{1}{\sqrt{N_{\text{Tx}} N_{\text{RIS}}}} \sum_{i=1}^{N_{\text{Tx}}} \sum_{l=1}^{N_{\text{RIS}}} \Theta_i \Xi_l \right. \\ \times \exp(-j2\pi c(r_{i,l} + r_{l,A})/f) \sqrt{\frac{A_{\text{RIS}} A}{8\pi^2 r_{\text{Tx,RIS}}^2 r_{\text{RIS,A}}^2}} \\ \left. \times \exp(-\frac{1}{2} \kappa_a(f) [r_{\text{Tx,RIS}} + r_{\text{RIS,A}}]) \right|^2 df dA, \quad (12)$$

where  $A_{\text{ave}}$  is the averaging area and  $A$  is the energy integration area. Notice that  $A_{\text{ave}}$  should not have an impact on the energy density, unless the energy through the area  $A$  is highly concentrated. Then smaller averaging area should be utilized for accurate average while observing the IEEE limits given above. In an ideal case with perfectly uniform energy density per unit area, we can calculate the ideal (worst case) energy density as

$$E_d = \int_B P_{\text{Tx}}(f) G_{\text{Tx}} G_{\text{RIS}} \frac{A_{\text{RIS}} \exp(-\kappa_a(f) [r_{\text{Tx,RIS}} + r_{\text{RIS,A}}])}{8\pi^2 r_{\text{Tx,RIS}}^2 r_{\text{RIS,A}}^2} df. \quad (13)$$

We will show in the numerical results that the IEEE reference levels can be reached, but those require very large RISs.

#### IV. NUMERICAL RESULTS

The numerical results are considered for the system model given in 1 and the assumptions therein. Unless otherwise stated, the simulations are based on parameters given in Table I and setup given in Fig. 2. That is, we keep the Tx stationary at direct line with RIS while altering the Rx position along radii 2, 5, and 10 meters around the RIS to maintain constant total distance per case while scanning all the possible Rx angles. The rest of the parameters were, while being rather optimistic to current communication systems, chosen to give the RIS the best chance to operate at high efficiency. The RISs are very promising technologies, but they need to be physically large compared to the wavelength to be able to redirect energy. At the same time, Tx and Rx need to be able to generate a lot of gain at +100 GHz frequencies. As such, the chosen parameters are not out of reach of future +100 GHz RIS deployments.

We will start from the beam squinting, as it will degrade the link quality quite a lot in all cases. Fig. 3 shows the

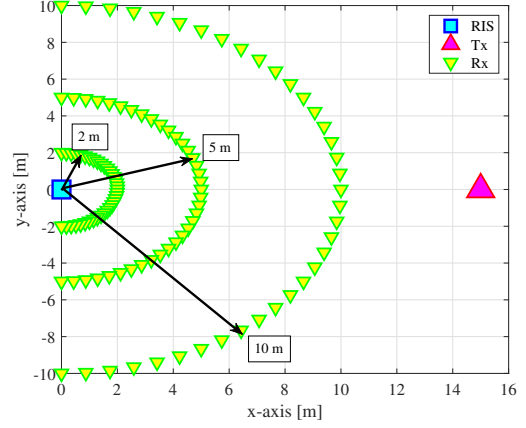


Fig. 2. Simulation model utilized in the numerical results. Tx is stationary at 15 meters away from the RIS and three Rx radii: 2, 5, and 10 meters with 37 Rx positions at each radius.

impact of the beam squinting on the frequency response as a function of the position of the Rx to the RIS. For this case the Tx was moved to 45 degree angle to RIS to better emphasize the superiority of the specular reflection. The natural reflection remains the perfect way to reflect energy as the required phase shifts in specular direction are zero across the reflecting surface. Hence, there is no beam squinting. The anomalous directions suffer from the beam squinting. The level of the beam squinting is dependent on the Tx and Rx antenna configurations, as well as RIS element configurations. Therefore, the signal degradation due to beam squinting is fully dependent on the system setup. We can see that the LPBF suffers very much at close proximity to RIS as it could be expected. The NFF gives much better energy levels, but even it cannot escape the beam squinting outside the specular reflection directions.

In the system setup herein, the beam squinting causes signal losses anywhere between 0 and about 8 dBs as we can see in Fig. 4 that gives the received average power levels over the Rx angles to RIS at three different Rx radii for NFF and LPBF with two different bandwidths. The narrow band naturally suffers less from the beam squinting as it is a wideband effect. The more interesting takeaway is the very optimistic theoretical gain. As it is untouched by the beam squinting due to narrow band assumption, it also gives maximum gain in all situations.

This is further evident in the frequency domain plots in Fig. 5 where we can see that the theoretical ideal result gives a flat frequency response while the full phase equations show major degradation in the frequency domain. The overall higher level of 2 GHz energy levels herein is due to we assume the total transmit energy is divided on the transmission band. Therefore, the energy density in frequency domain is higher with 2 GHz band than 10 GHz. The total energies are the same. Hence, the peak energies in Fig. 4 are the same for both bandwidths even if the narrow bandwidth in general gives more received power.

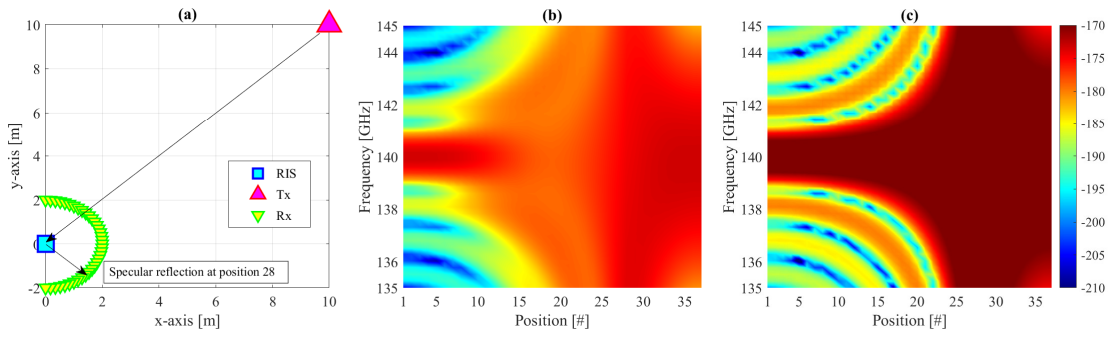


Fig. 3. (a) Illustration of the beam squinting with Tx at coordinates (10, 10) and Rx radius 2 meters. (b) Received energy as a function of frequency and user position for linear phase beamformer. (c) Same as (b) for near field focusing.

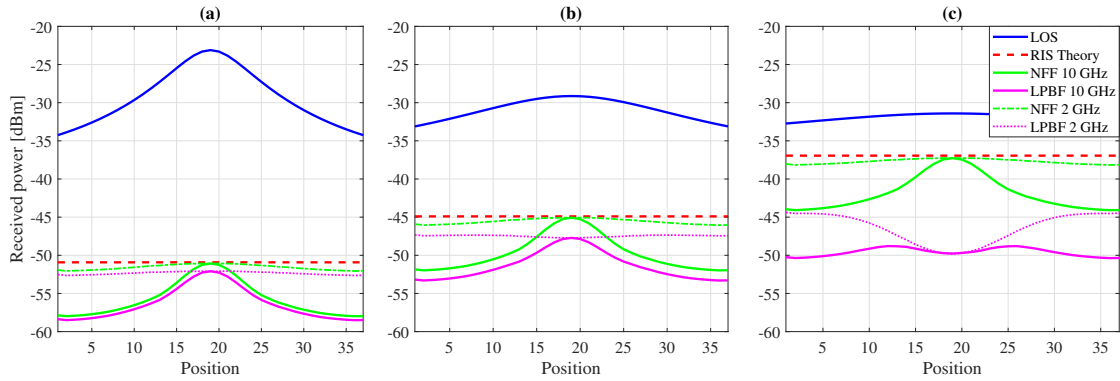


Fig. 4. Average received power over frequency as a function of the Rx position for distances (a) 10 meters, (b) 5 meters, and (c) 2 meters.

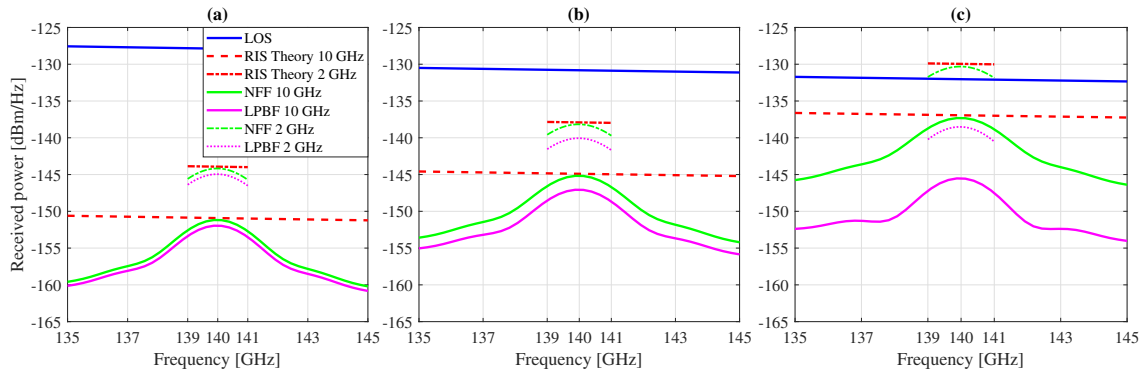


Fig. 5. Average received power over Rx positions as a function of frequency for distances (a) 10 meters, (b) 5 meters, and (c) 2 meters, and for 10 and 2 GHz bandwidths.

Finally, let us look into the potential health implications of very large RISs. Fig. 6 gives the received energy densities as a function of the unit area distance from the RIS. The three subfigures give the energy densities for the following Tx and RIS setups: (a)  $32 \times 32$  RIS,  $\lambda/2$  patch sizes, and  $8 \times 8$  Tx, (b)  $32 \times 32$  RIS,  $2\lambda$  patch sizes, and  $8 \times 8$  Tx, and (c)  $64 \times 64$  RIS,  $2\lambda$  patch sizes, and  $16 \times 16$  Tx. Black lines give the IEEE ERLs and the blue line gives the Tx energy density at the equivalent distance to Rx distance in the figures. We also give the results for LPBF and NFF. Firstly, we can see that the RIS needs to be very large to be able to impose harmful energy densities. It is still possible in some isolated applications where

RIS would be very large and close to users. However, these applications are most likely beyond 6G in the horizon at the time of writing this paper. Second observation is that the very high energy densities require near field focusing. Lastly, in Fig. 6 (c) we see that the theoretical extreme value is slightly above the full phase model. This follows from the fact that the RIS is concentrating the energy into very small area. The averaging should be made over even smaller than  $1 \text{ cm}^2$  area to keep up with the theory. This is not all positive, as it hints that the local energy densities are very high.

The results herein give an image of difficult near field that can be tamed with proper beamforming. The NFF is a powerful

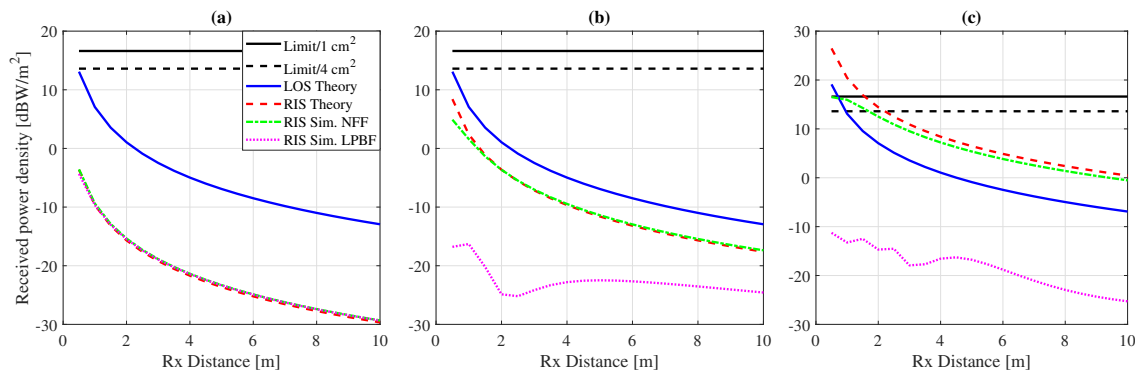


Fig. 6. Energy density close to RIS with safety limits, i.e., about 13.6 dBW/m<sup>2</sup> for 4 cm<sup>2</sup> energy averaging area and 16.6 dBW/m<sup>2</sup> for 1 cm<sup>2</sup>. (a) 32×32 RIS,  $\lambda/2$  patch sizes, and 8×8 Tx, (b) 32×32 RIS,  $2\lambda$  patch sizes, and 8×8 Tx, and (c) 64×64 RIS,  $2\lambda$  patch sizes, and 16×16 Tx.

beamforming method in the near field, but requires one extra degree of freedom that can be challenging in above 100 GHz frequencies. However, when done right, the near field offers large amounts of gain if the system can cope with the losses coming from the beam squinting.

## V. CONCLUSION

We analysed the near field performance of RISs in this paper. It was shown that the near field of the RIS can offer very large gains if one can align the array phases at the Rx locations. This imposes a problem of estimating the third required degree of freedom, the distance to solve the exact locations. Regardless of the beamforming, wideband signals tend to suffer from beam squinting arising from the non-ideal beam steering phases across large bandwidths. This leads to channel losses especially in the case of passive RISs that have limited means to counter the beam squinting. It was also concluded that RISs, even large ones, are mostly safe to approach by humans due to large losses in reflection type communications. Still, caution should be advised in the future system utilizing extremely large RISs with thousands of reflecting elements. In any near future scenarios, the RISs are perfectly harmless to living creatures, and they can be very useful for maximizing the signal levels in complex propagation environments.

## ACKNOWLEDGEMENT

This work was supported by the Horizon 2020, European Union’s Framework Programme for Research and Innovation, under grant agreement no. 871464 (ARIADNE). It was also supported in part by the Academy of Finland 6Genesis Flagship. On top of these, the trip to the ISMICT’2023 conference and the related research visit to University of Nebraska-Lincoln were further supported by EU Horizon 2020 Marie Skłodowska-Curie Actions ROVER project and Finnish-American Innovation Accelerator FARIA.

## REFERENCES

[1] M. Latva-Aho and K. Leppänen, Eds., *Key drivers and research challenges for 6G ubiquitous wireless intelligence*, ser. 6G research visions. University of Oulu, Sep. 2019, no. 1.

[2] I. F. Akyildiz, J. M. Jornet, and C. Han, “Terahertz band: Next frontier for wireless communications,” *Elsevier Phys. Commun.*, vol. 12, pp. 16–32, Sep. 2014.

[3] J. M. Jornet and I. F. Akyildiz, “Channel modeling and capacity analysis for electromagnetic nanonetworks in the terahertz band,” *IEEE Trans. Wireless Commun.*, vol. 10, no. 10, pp. 3211–3221, Oct. 2011.

[4] M. Di Renzo, A. Zappone, M. Debbah, M. S. Alouini, C. Yuen, J. de Rosny, and S. Tretyakov, “Smart radio environments empowered by reconfigurable intelligent surfaces: How it works, state of research, and the road ahead,” *IEEE Journal on Selected Areas in Communications*, vol. 38, no. 11, pp. 2450–2525, 2020.

[5] R. Schroeder, J. He, and M. Juntti, “Passive ris vs. hybrid ris: A comparative study on channel estimation,” in *IEEE VTC2021-Spring*, 2021, pp. 1–7.

[6] D. Acharya, J. Kokkonen, A. Pärssinen, and M. Berg, “Performance comparison of near-field focused and conventional phased antenna arrays at 140 GHz,” in *Proc. EuCNC 6G Summit*, 2021, pp. 1–6.

[7] J. Kokkonen and M. Juntti, “Channel modeling for reflective phased array type riss in mmwave networks,” in *Proc. ACM mmNets*, 2021, p. 31–36.

[8] —, “Stochastic geometry based interference analysis of multiuser mmWave networks with RIS,” in *Proc. IEEE PIMRC*, Sept. 2021, pp. 1–6.

[9] W. Tang, M. Z. Chen, X. Chen, J. Y. Dai, Y. Han, M. Di Renzo, Y. Zeng, S. Jin, Q. Cheng, and T. J. Cui, “Wireless communications with reconfigurable intelligent surface: Path loss modeling and experimental measurement,” *Trans. Wireless. Comm.*, vol. 20, no. 1, p. 421–439, jan 2021.

[10] E. Basar and I. Yildirim, “Indoor and outdoor physical channel modeling and efficient positioning for reconfigurable intelligent surfaces in mmWave bands,” *arXiv: 2006.02240*, pp. 1–10, 2020.

[11] O. Özdogan, E. Björnson, and E. G. Larsson, “Intelligent reflecting surfaces: Physics, propagation, and pathloss modeling,” *arXiv:1911.03359*, pp. 1–5, 2019.

[12] F. H. Danufane, M. Di Renzo, J. de Rosny, and S. Tretyakov, “On the path-loss of reconfigurable intelligent surfaces: An approach based on Green’s theorem applied to vector fields,” *arXiv: 2007.13158*, pp. 1–30, 2020.

[13] A.-A. A. Boulogeorgos and A. Alexiou, “Pathloss modeling of reconfigurable intelligent surface assisted THz wireless systems,” *arXiv: 2102.08757*, pp. 1–6, 2021.

[14] J. Kokkonen, J. Lehtomäki, and M. Juntti, “A line-of-sight channel model for the 100–450 gigahertz frequency band,” *EURASIP J. Wireless Commun. Netw.*, vol. 88, pp. 1–15, 2021.

[15] N. T. Nguyen, J. Kokkonen, and M. Juntti, “Beam Squint Effects in THz Communications with UPA and ULA: Comparison and Hybrid Beamforming Design,” in *Proc. IEEE Globecom Workshops (GC Wkshps)*, 2022, pp. 1754–1759.

[16] “IEEE Standard for Safety Levels with Respect to Human Exposure to Electric, Magnetic, and Electromagnetic Fields, 0 Hz to 300 GHz,” *IEEE Std C95.1-2019*, pp. 1–312, 2019.